Available online at www.sciencedirect.com
ScienceDirect
Trans. Nonferrous Met. Soc. China 31(2021) 512−520
Transactions of Nonferrous Metals Society of China
www.tnmsc.cn

Effects of La on microstructure and mechanical properties of $NbMoTiVSi_{0.2}$ refractory high entropy alloys

Qin XU[1], De-zhi CHEN[2], Cong-rui WANG[1], Wen-chao CAO[2],
Qi WANG[2], Hong-zhi CUI[3], Shu-yan ZHANG[4], Rui-run CHEN[2,3]

1. School of Mechanic and Electrical Engineering, Henan University of Technology, Zhengzhou 450001, China;
2. National Key Laboratory for Precision Hot Processing of Metals,
Harbin Institute of Technology, Harbin 150001, China;
3. School of Materials Science and Engineering,
Shandong University of Science and Technology, Qingdao 266590, China;
4. Centre of Excellence for Advanced Materials, Dongguan 523808, China

Received 29 March 2020; accepted 18 December 2020

Abstract: To study the effects of La on the microstructure and mechanical properties of refractory high entropy alloys, $NbMoTiVSi_{0.2}$ alloys with different La contents were prepared. Phase constitution, microstructure evolution, compressive properties and related mechanisms were systematically studied. Results show that the alloys with La addition are composed of BCC solid solution, eutectic structure, MSi_2 disilicide phase and La-containing precipitates. Eutectic structure and most of La precipitates are formed at the grain boundaries. Disilicide phase is formed in the grains. La can change the grain morphologies from dendritic structure to near-equiaxed structure, and the average grain size decreases from 180 to 20 μm with the increase of La content from 0 to 0.5 at.%. Compressive testing shows that the ultimate strength and the yield strength increase with the increase of La content, which is resulted from the grain boundary strengthening. However, they cannot be greatly improved because of the formation of MSi_2 disilicide phase with low strength. The ductility decreases with the increase of La content, which is due to the La precipitates and brittle MSi_2 disilicide phase.

Key words: high entropy alloy; lanthanum; eutectic structure; refractory metal; disilicide phase

1 Introduction

High entropy alloys (HEAs) containing at least five principal elements were first put forward in 2004 [1,2]. They have attracted much attention due to their high thermal stability and excellent mechanical properties [3−6]. HEAs were originally defined as homogeneous solid solutions with a single BCC, FCC or HCP crystal structure. Among them, refractory high entropy alloys (RHEAs) with BCC solid solution structure are the most potential candidates for high temperature structural applications [6−9]. RHEAs are composed of refractory elements such as W, Ta, Nb, Mo, Hf, Zr, Ti and V, and are designed in equimolar or near equimolar ratios [10−14]. Due to the high melting point, RHEAs show high strength and excellent performance at high temperatures.

The purpose of designing RHEAs is to extend the service temperature of structural materials, and most of RHEAs show the potential to extend the service temperature of blades and disks beyond current superalloys. Many RHEAs such as $Al_{0.4}Hf_{0.6}NbTaTiZr$, $AlMo_{0.5}NbTa_{0.5}TiZr$ and $NbTiVTaAl_x$ (x=0−1, molar ratio) have sufficient

Corresponding author: Rui-run CHEN; Tel/Fax: +86-451-86412394; E-mail: ruirunchen@hit.edu.cn
DOI: 10.1016/S1003-6326(21)65513-9

room-temperature compressive ductility ($\varepsilon \geq 10\%$), but there is a degree of cleavage fracture [15,16]. Other refractory high entropy alloys (AlNbTiV [17], HfMoNbTiZr [18], AlNbTiZr [19] and NbMoTiV [20]) have attractive yield strength with good enough ductility, which can be further improved by alloy composition modification and microstructure control. LIU et al [21] reported that $HfMo_{0.5}NbTiV_{0.5}Si_x$ can achieve excellent strength at elevated temperature and reasonable ductility at room temperature by adding silicon. Many investigations have confirmed that the addition of rare earth element La can refine the microstructure of steel, TiAl and many other alloys [22−28], thus improve their mechanical properties. However, to the best of our knowledge, the effects of La on the microstructure and mechanical properties of RHEAs have not been studied.

Previous study [20] showed that $NbMoTiVSi_{0.2}$ refractory high entropy alloy exhibited good room-temperature compressive ductility (ε >16%) and high yield strength ($\sigma_{0.2}$>1760 MPa). In this study, the $NbMoTiVSi_{0.2}$ refractory high entropy alloys were modified by adding different contents of La, and the alloys were prepared by vacuum arc melting process. The effects of rare element La on the phase constitution, microstructure evolution, mechanical properties and the related mechanisms were thoroughly studied.

2 Experimental

The raw materials were sponge titanium (purity ≥99.98%), niobium sheet (purity ≥99.98%), molybdenum block (purity ≥99.98%), vanadium block (purity ≥99.98%), particle silicon (purity ≥99.98%) and lanthanum powder (purity ≥99.99%). The $NbMoTiVSi_{0.2}$ refractory high entropy alloys with different La contents (0, 0.1, 0.2, 0.3, 0.4, and 0.5 at.%) were prepared by the vacuum non-consumable arc melting with tungsten electrode. Before melting, the furnace was evacuated to 3×10^{-3} Pa and filled with argon as protective atmosphere, and then the alloys were melted into button ingots. The ingots were melted 5 times to ensure the composition homogeneity.

Specimens with dimensions of 10 mm × 10 mm × 8 mm were cut from the ingots by electrical-discharge wire cutting. After grinding and polishing, phase analysis and microstructure observation were carried out. The crystal structure of the alloys was identified by X-ray diffractometry (XRD, Panalytical Empyrean) with Cu K_α radiation, and the scanning angle (2θ) ranged from 20° to 90° with a scanning rate of 8 (°)/min. Scanning electron microscopy (SEM, FEI, Quanta 200FEG) was used to observe the microstructure morphology in the backscatter electron (BSE) mode. The compositions of different phases were examined by energy dispersion spectroscopy (EDS). The average grain size of alloys was quantified by linear intercept method with Image-Pro Plus software. Compressive testing was conducted at room temperature with an Instron 5569 universal tester. The samples with sizes of d4 mm × 6 mm were tested with an initial strain rate of 1×10^{-3} s^{-1}, and at least 3 samples were tested for each alloy.

3 Results and discussion

3.1 Phase constitution of $(NbMoTiVSi_{0.2})_{100-x}La_x$ alloys

Figure 1 shows the XRD patterns of alloys $(NbMoTiVSi_{0.2})_{100-x}La_x$ (x is molar fraction, %). The results show that the crystal structure of the $NbMoTiVSi_{0.2}$ alloy without La is composed of BCC solid solution and silicide phase M_5Si_3 (M=Nb,Mo,Ti,V). The $(NbMoTiVSi_{0.2})_{99.9}La_{0.1}$, $(NbMoTiVSi_{0.2})_{99.8}La_{0.2}$ and $(NbMoTiVSi_{0.2})_{99.7}La_{0.3}$ alloys are also composed of BCC solid solution and M_5Si_3 silicide phase. When the La addition is

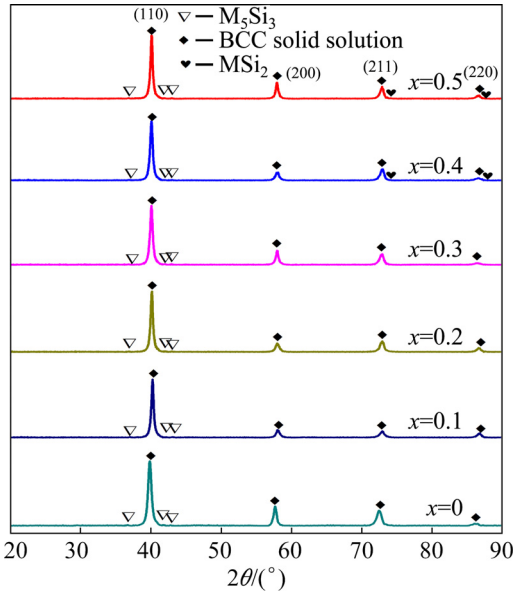

Fig. 1 XRD patterns of $(NbMoTiVSi_{0.2})_{100-x}La_x$ alloys

increased to 0.4 and 0.5 at.%, the disilicide phase MSi_2(M=Mo,Nb,Ti,V) appeared in XRD patterns. Therefore, the $(NbMoTiVSi_{0.2})_{99.6}La_{0.4}$ and $(NbMoTiVSi_{0.2})_{99.5}La_{0.5}$ alloys are composed of BCC solid solution, M_5Si_3 silicide phase and MSi_2 disilicide phase.

Besides, the peaks of BCC phase shift slightly to the higher 2θ direction with the increase of La content, which shows the decrease of the lattice parameters of BCC phase. This change is resulted from the bigger atomic radius of La (2.740 Å) compared with that of the other alloying elements (shown in Table 1). Furthermore, the diffraction peaks of the BCC phase become shorter after adding La element, which indicates that the amount of the BCC phase decreases with the increase of La content.

The diffraction peaks of M_5Si_3 silicide phase for the $NbMoTiVSi_{0.2}$ alloy are much stronger than those of the alloys with La. This indicates that the addition of La can decrease the amount of silicide phase in the studied alloys. When the addition of La is higher than 0.4 at.%, the amount of the silicide phase will decrease and the disilicide phase will be formed.

3.2 Microstructures of $(NbMoTiVSi_{0.2})_{100-x}La_x$ alloys

Figures 2 and 3 show the microstructures of the $(NbMoTiVSi_{0.2})_{100-x}La_x$ alloys with different magnifications. Figure 4 shows the positions for EDS measurement of $(NbMoTiVSi_{0.2})_{99.9}La_{0.1}$ alloy with higher magnification. The results in Figs. 2−4 show that there are five different phases in the alloys after adding different contents of La. They are the light gray phase and the black phase at the grain boundaries, the dark grey phase, the white phase and the black phase in the light grey phase. These phases were examined by EDS, and the results are summarized in Table 2. Combining the XRD and EDS results, it is clear that the light gray phase marked with *A* in Fig. 4 is the primary BCC solid solution, which is the matrix, the black phase marked with *B* is M_5Si_3 silicide phase, the dark grey phase marked with *C* is the eutectic BCC solid solution, the white phase marked with *D* is the precipitate that is rich in La, and the black phase marked with *E* is the MSi_2 disilicide phase that is formed in the grains of the alloy (rich in Mo). However, the MSi_2 disilicide phase cannot be detected by X-ray diffraction (XRD) in $(NbMoTiVSi_{0.2})_{99.9}La_{0.1}$, $(NbMoTiVSi_{0.2})_{99.8}La_{0.2}$ and $(NbMoTiVSi_{0.2})_{99.7}La_{0.3}$ alloys because the volume fraction is too low.

Phases in Fig. 4 show that eutectic structure is composed of eutectic BCC solid solution (dark grey phase marked with *C*) and M_5Si_3 silicide phase (black phase marked with *B*) formed at the grain boundaries. Most of the La precipitates are also formed at the grain boundaries, especially at the interface of the silicide phase and the primary BCC solid solution (shown in Fig. 3). The MSi_2 disilicide phases with irregular shape are formed in the primary BCC phase by addition of La. Therefore, the $(NbMoTiVSi_{0.2})_{100-x}La_x$ alloys with addition of La consist of primary BCC solid solution, eutectic structure, La precipitates and MSi_2 disilicide phase. With the increase of La addition, more La precipitates and MSi_2 disilicide phase are formed, but the size of MSi_2 disilicide phase is almost not changed.

The microstructure of the $NbMoTiVSi_{0.2}$ alloy shows typical dendritic morphology (shown in Fig. 2(a)), and the average grain size is about 180 μm. The grains of the alloys are refined after adding La, and the morphology changes from the dendritic structure to near-equiaxed structure. The eutectic structure is also formed at the grain

Table 1 Physical properties of elements in studied alloys

Element	Atomic number	Molar mass/ ($g\cdot mol^{-1}$)	Melting temperature/ °C	Density/ ($g\cdot cm^{-3}$)	Atomic radius/ Å
Nb	41	92.92	2468	8.57	1.429
Mo	42	95.94	2610	10.22	1.363
Ti	22	47.87	1670	4.5	1.462
V	23	50.94	1890	5.96	1.316
Si	14	28.09	1410	2.33	1.153
La	57	138.9	921	6.15	2.740

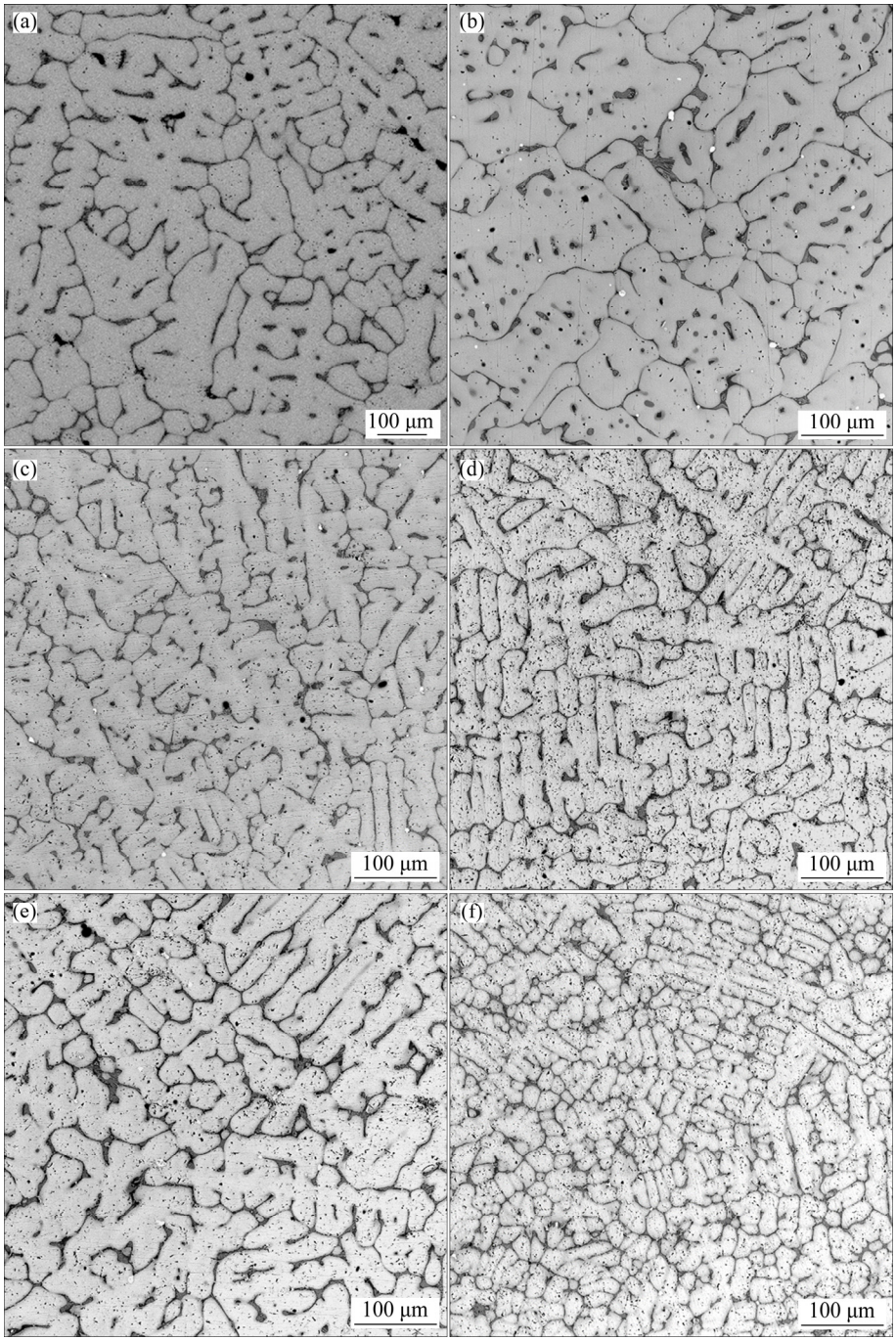

Fig. 2 Microstructures of $(NbMoTiVSi_{0.2})_{100-x}La_x$ alloys with lower magnifications: (a) x=0; (b) x=0.1; (c) x=0.2; (d) x=0.3; (e) x=0.4; (f) x=0.5

boundaries of the $(NbMoTiVSi_{0.2})_{100-x}La_x$ alloys. The eutectic structure of the alloys is also refined by the addition of La. The average grain size of the alloy decreases with the increase of La content (shown in Fig. 5). The average grain size is the smallest in the alloys when the addition of La is 0.5 at.%, which is 20 μm.

The addition of rare earth element can effectively affect the nucleation rate of the melt and the subsequent growth of the nucleus. According the classical nucleation theory [29,30], the addition of rare earth element La reduces the surface tension at the phase interface and the energy fluctuation required to generate crystal nucleus. Consequently, the nucleation rate of the $NbMoTiVSi_{0.2}$ alloy melt can be improved by the addition of La. Meanwhile, the rare earth oxides at the frontier of the solid/liquid interface are ultra-micro particles, and

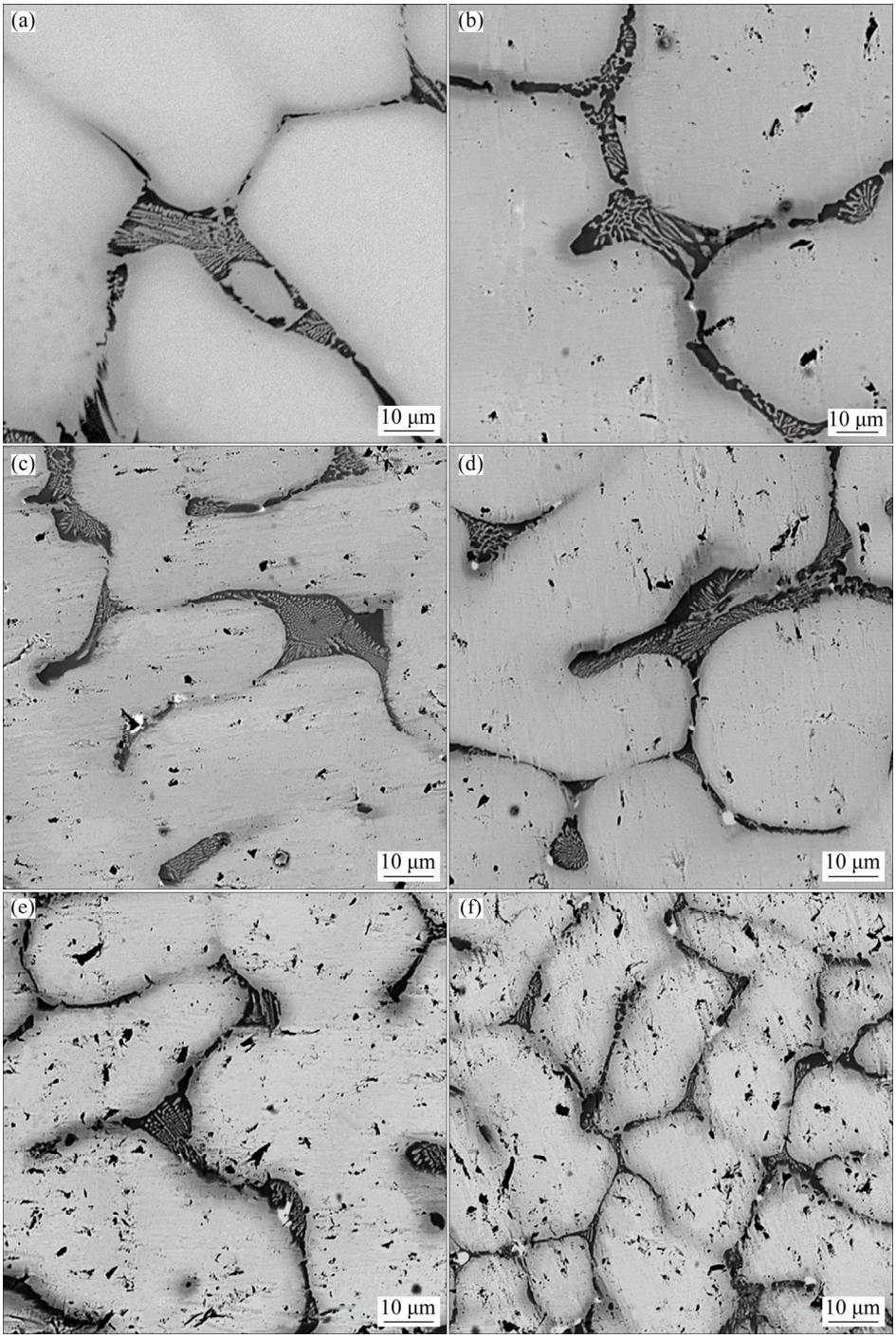

Fig. 3 Microstructures of $(NbMoTiVSi_{0.2})_{100-x}La_x$ alloys with higher magnifications: (a) x=0; (b) x=0.1; (c) x=0.2; (d) x=0.3; (e) x=0.4; (f) x=0.5

their melting points are higher. They can prevent the growth of crystals and the movement of the grain boundaries, thus the grains and the eutectic structure of the $(NbMoTiVSi_{0.2})_{100-x}La_x$ alloys are refined.

The addition of rare earth element into Nb−Si alloys can propel the formation of $NbSi_2$ disilicide phase from Nb_5Si_3 silicide phase [31], and the phase transformation from Nb_5Si_3 silicide phase to $NbSi_2$ disilicide phase during cooling leads to the formation of microcracks [32,33]. In this study, the addition of La can lead to the formation of MSi_2 disilicide phase distributing in the primary BCC solid phase, and the amount of the MSi_2 disilicide phase increases with the increase of La addition.

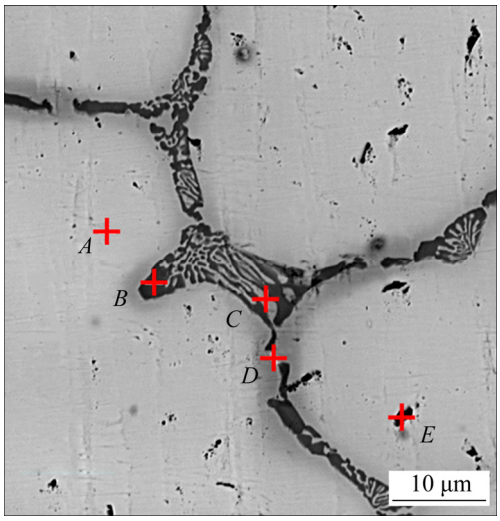

Fig. 4 Positions for EDS measurement of $(NbMoTiVSi_{0.2})_{99.9}La_{0.1}$ alloy with higher magnification

Table 2 EDS results of five positions in Fig. 4

Position	Content/at.%					
	Nb	Mo	Ti	V	Si	La
A	25.64	35.36	17.35	18.2	2.42	1.04
B	18.03	3.09	33.47	8.77	36.06	0.59
C	21.34	14.35	28.10	23.45	11.91	0.86
D	14.08	8.74	14.99	14.36	7.63	40.20
E	8.97	13.50	5.61	6.22	65.61	0.09

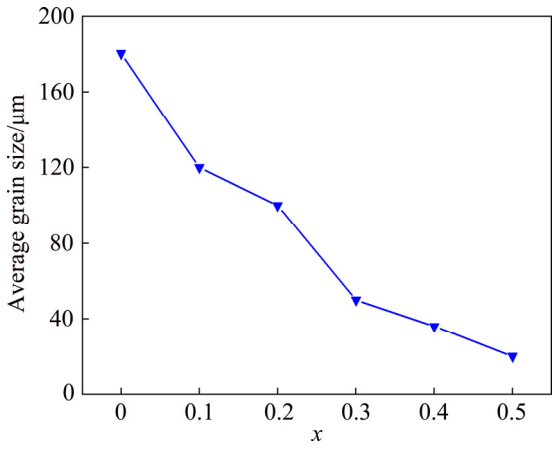

Fig. 5 Average grain size of $(NbMoTiVSi_{0.2})_{100-x}La_x$ alloys

3.3 Mechanical properties of $(NbMoTiVSi_{0.2})_{100-x}La_x$ alloys

The compressive stress−strain curves of $(NbMoTiVSi_{0.2})_{100-x}La_x$ alloys are shown in Fig. 6, and the fracture strain, ultimate strength and yield strength of the alloys are summarized in Table 3.

The results show that the ultimate strength of the alloys with different additions of La ranges from 2085 to 2157 MPa. The yield strength of the alloys ranges from 1766 to 1929 MPa. The ultimate strength of the alloys increases with increasing addition of La except the $(NbMoTiVSi_{0.2})_{99.6}La_{0.4}$ alloy, and yield strength of the alloys increases by addition of La. Both the ultimate strength and yield strength of $(NbMoTiVSi_{0.2})_{99.5}La_{0.5}$ alloy are the highest. The ultimate strength and yield strength of $(NbMoTiVSi_{0.2})_{99.5}La_{0.5}$ alloy are 2157 and 1929 MPa, respectively. The yield strength of $(NbMoTiVSi_{0.2})_{99.5}La_{0.5}$ alloy is increased by 9.3% compared with that of $NbMoTiVSi_{0.2}$ alloy. The ultimate strength of $(NbMoTiVSi_{0.2})_{99.6}La_{0.4}$ alloy is the lowest (2085 MPa).

The fracture strains of the $(NbMoTiVSi_{0.2})_{100-x}La_x$ alloys decreases with the addition of La. The fracture strain of $NbMoTiVSi_{0.2}$ alloy is 16.47%. The fracture strain of $(NbMoTiVSi_{0.2})_{99.6}La_{0.4}$ alloy decreases to 12.83%, and that of the $(NbMoTiVSi_{0.2})_{99.5}La_{0.5}$ alloy with the highest ultimate and yield strengths is 15.28%.

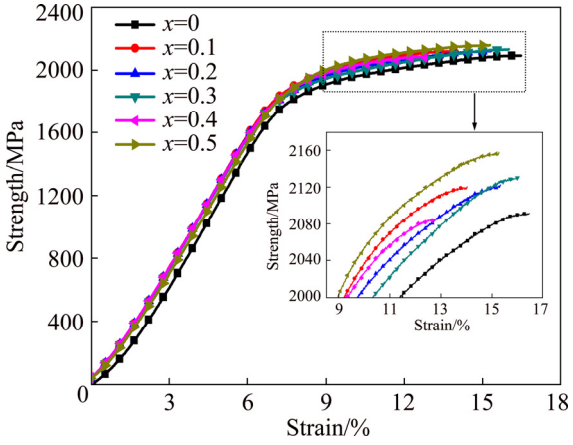

Fig. 6 Compressive strength−strain curves of $(NbMoTiVSi_{0.2})_{100-x}La_x$ alloys

Table 3 Mechanical properties of $(NbMoTiVSi_{0.2})_{100-x}La_x$ alloys

x	Ultimate strength/MPa	Yield strength/MPa	Fracture strain/%
0	2091	1766	16.47
0.1	2120	1868	14.03
0.2	2122	1814	15.34
0.3	2130	1839	16.00
0.4	2085	1828	12.83
0.5	2157	1929	15.28

As has been stated above, the addition of La to $NbMoTiVSi_{0.2}$ alloys can prevent the growth of crystals and the movement of the grain boundaries, and refine the grains of the $NbMoTiVSi_{0.2}$ alloys. Therefore, the mechanical properties of the $NbMoTiVSi_{0.2}$ alloys can be improved by the addition of La for the grain boundary strengthening effect.

The addition of La to the $NbMoTiVSi_{0.2}$ alloys leads to the formation of MSi_2 disilicide phase, which is distributed in the primary BCC phase. However, the transformation from Nb_5Si_3 silicide phase to $NbSi_2$ disilicide phase during cooling can result in the formation of microcracks. The strength of $MoSi_2$ phase is only 350 MPa [33]. Thus, the strength of $NbMoTiVSi_{0.2}$ alloy cannot be greatly improved due to the lower strength MSi_2 disilicide phase.

La precipitates appear in $NbMoTiVSi_{0.2}$ alloy by addition of La, and the amount of La precipitates increases with the increase of La content. The La precipitates distributed at the grain boundaries lead to stress concentration during testing. Consequently, the La precipitates and the brittle MSi_2 disilicide phase bring about the brittle fracture and reduce the ductility of alloys.

Therefore, the ultimate strength of $NbMoTiVSi_{0.2}$ alloys can be improved by adding rare earth element La, which is attributed to the grain boundary strengthening effect. However, the strength of the alloy cannot be greatly improved due to the formation of low strength MSi_2 disilicide phase. But the fracture strain and the ductility of the alloys decrease because of the La precipitates distributed at the grain boundaries and the formation of brittle MSi_2 disilicide phase.

4 Conclusions

(1) The microstructure of $(NbMoTiVSi_{0.2})_{100-x}La_x$ RHEAs with different La contents consists of primary BCC solid solution phase, eutectic structure, disilicide phase MSi_2 (M=Mo, Nb, Ti and V) and La precipitates. Eutectic structure and most of La precipitates are formed at grain boundaries, and the disilicide phases are distributed in the primary BCC solid solution.

(2) The La precipitates and disilicide phase are formed in the $(NbMoTiVSi_{0.2})_{100-x}La_x$ RHEAs when La is added, and their contents increase with the increase of La content.

(3) The grains of $(NbMoTiVSi_{0.2})_{100-x}La_x$ RHEAs are refined by adding La. With the increase of La content, the grain morphology is changed from dendritic structure to near-equiaxed structure. The average grain size of the alloys decreases with the increase of La content, and the average grain size of $(NbMoTiVSi_{0.2})_{99.5}La_{0.5}$ alloy is the smallest (20 μm).

(4) The ultimate strength and the yield strength of the $(NbMoTiVSi_{0.2})_{100-x}La_x$ RHEAs increase with the increase of La content, which is resulted from the grain boundary strengthening. But they cannot be greatly improved due to the formation of low strength disilicide phase. The ductility is reduced because of the La precipitates and the brittle disilicide phase.

Acknowledgments

The authors are grateful for the financial supports from the National Natural Science Foundation of China (51825401 and 52001114), the State Key Laboratory of Materials Processing and Die & Mould Technology (P2020-023) and the Guangdong Introducing Innovative and Entrepreneurial Teams, China (2016ZT06G025).

References

[1] YEH J W, CHEN S K, LIN S J, GAN J Y, CHIN T S, SHUN T T, TSAU C H, CHANG S Y. Nanostructured high-entropy alloys with multiple principal elements: Novel alloy design concepts and outcomes [J]. Advanced Engineering Materials, 2004, 6(5): 299−303.

[2] SHABANI A, TOROGHINEJAD M R. Evaluation of microstructure and texture formation during annealing of cold-rolled FeCrCuMnNi multiphase high-entropy alloy [J]. Transactions of Nonferrous Metals Society of China, 2020, 30(2): 449−462.

[3] GAO N, LU D H, ZHAO Y Y, LIU X W, LIU G H, WU Y, LIU G, FAN Z T, LU Z P, GEORGE E P. Strengthening of a CrMnFeCoNi high-entropy alloy by carbide precipitation [J]. Journal of Alloys and Compounds, 2019, 792: 1028−1035.

[4] ZHENG Hui-ting, CHEN Rui-run, QIN Gang, LI Xin-zhong, FU Heng-zhi. Microstructure evolution, Cu segregation and tensile properties of CoCrFeNiCu high entropy alloy during directional solidification [J]. Journal of Materials Science & Technology, 2020, 38: 19−27.

[5] FU Jian-xin, CAO Cheng-ming, TONG Wei, PENG Liang-ming. Effect of thermomechanical processing on microstructure and mechanical properties of CoCrFeNiMn high entropy alloy [J]. Transactions of Nonferrous Metals Society of China, 2018, 28(5): 931−938.

[6] QIN G, CHEN R R, LIAW P K, GAO Y F, LI X Q, ZHENG

H T, WANG L, SU Y Q, GUO J J, FU H Z. A novel face-centered-cubic high-entropy alloy strengthened by nanoscale precipitates [J]. Scripta Materialia, 2019, 172: 51−55.

[7] CAO Yuan-kui, LIU Yong, LIU Bin, ZHANG Wei-dong, WANG Jia-wen, DU Meng. Effects of Al and Mo on high temperature oxidation behavior of refractory high entropy alloys [J]. Transactions of Nonferrous Metals Society of China, 2019, 29(7):1476−1483.

[8] ZHU Cheng-long, LI Zhan-jiang, HONG Chun-fu, DAI Ping-qiang, CHEN Jun-feng. Microstructure and mechanical properties of the TiZrNbMoTa refractory high-entropy alloy produced by mechanical alloying and spark plasma sintering [J]. International Journal of Refractory Metals and Hard Materials, 2020, 93: 105357.

[9] MIRACLE D B, TSAI M H, SENKOV O N, SONI V, BANERJEE R. Refractory high entropy superalloys (RSAs) [J]. Scripta Materialia, 2020, 187: 445−452.

[10] YAO J Q, LIU X W, GAO N, JIANG Q H , LI N, LIU G, ZHANG W B, FAN Z T. Phase stability of a ductile single-phase BCC $Hf_{0.5}Nb_{0.5}Ta_{0.5}Ti_{1.5}Zr$ refractory high-entropy alloy [J]. Intermetallics, 2018, 98: 79−88.

[11] LIU Qing, WANG Guo-feng, SUI Xiao-chong, LIU Yong-kang, YANG Jian-lei . Microstructure and mechanical properties of ultra-fine grained MoNbTaTiV refractory high-entropy alloy fabricated by spark plasma sintering [J]. Journal of Materials Science & Technology, 2019, 35: 2600−2607.

[12] TIAN Fu-yang, WANG Dong-ping, SHEN Jiang, WANG Yang. An ab initio investigation of ideal tensile and shear strength of TiVNbMo high-entropy alloy [J]. Materials Letters, 2016, 166: 271−275.

[13] MARESCA F, CURTIN W A. Mechanistic origin of high strength in refractory BCC high entropy alloys up to 1900 K [J]. Acta Materialia, 2020, 182: 235−249.

[14] COUZINIÉ J P, DIRRAS G, PERRIÈRE L, CHAUVEAU T, LEROY E, CHAMPION Y, GUILLOT I. Microstructure of a near-equimolar refractory high-entropy alloy [J]. Materials Letters, 2014, 126: 285−287.

[15] SENKOV O N, SENKOVA S V, WOODWARD C. Effect of aluminum on the microstructure and properties of two refractory high-entropy alloys [J]. Acta Materialia, 2014, 68: 214−228.

[16] YANG X, ZHANG Y, LIAW P K. Microstructure and compressive properties of $NbTiVTaAl_x$ high entropy alloys [J]. Procedia Engineering, 2012, 36: 292−298.

[17] STEPANOV N D, SHAYSULTANOV D G, SALISHCHEV G A, TIKHONOVSKY M A. Structure and mechanical properties of a light-weight AlNbTiV high entropy alloy [J]. Materials Letters, 2015, 142: 153−155.

[18] GUO N N, WANG L, LUO L S, LI X Z, SU Y Q, GUO J J, FU H Z. Microstructure and mechanical properties of refractory MoNbHfZrTi high-entropy alloy [J]. Materials & Design, 2015, 81: 87−94.

[19] JAYARAJ J, THIRATHIPVIWAT P, HAN J, GEBERT A. Microstructure, mechanical and thermal oxidation behavior of AlNbTiZr high entropy alloy [J]. Intermetallics, 2018, 100: 9−19.

[20] XU Qin, CHEN De-zhi, TAN Chong-yang, BI Xiao-qin, WANG Qi, CUI Hong-zhi, CHEN Rui-run. $NbMoTiVSi_x$ refractory high entropy alloys strengthened by forming BCC phase and silicide eutectic structure [J]. Journal of Materials Science & Technology, 2021, 60: 1−7.

[21] LIU Yuan, ZHANG Yan, ZHANG Heng, WANG Nai-juan, CHEN Xiang, ZHANG Hua-wei, LI Yan-xiang. Microstructure and mechanical properties of refractory $HfMo_{0.5}NbTiV_{0.5}Six$ high-entropy composites [J]. Journal of Alloys and Compounds, 2016, 694: 869−876.

[22] BAGABER S A, ABDULLAHI T, HARUN Z, DAIB N, OTHMAN M H D. The effect of lanthanum addition on the microstructure and mechanical properties of A390 aluminium alloy [J]. Arabian Journal for Science and Engineering, 2017, 42(11): 4559−4564.

[23] CHEN Yan, CHENG Ming, SONG Hong-wu, ZHANG Shi-hong, LIU Jin-song, ZHU Yan. Effects of lanthanum addition on microstructure and mechanical properties of as-cast pure copper [J]. Journal of Rare Earths, 2014, 32(11): 1056−1063.

[24] HAMIDZADEH M A, MERATIAN M, SAATCHI A. Effect of cerium and lanthanum on the microstructure and mechanical properties of AISI D2 tool steel [J]. Materials Science and Engineering A, 2013, 571: 193−198.

[25] HADI M, MERATIAN M, SHAFYEI A. The effect of lanthanum on the microstructure and high temperature mechanical properties of a beta-solidifying TiAl alloy [J]. Journal of Alloys and Compounds, 2015, 618: 27−32.

[26] LI Wen-hu, ZHANG Guo-jun, AI Tao-tao, LI Rui. Design and mechanical properties of Mo−10Si−7B alloys doped with lanthanum oxide by a hot pressing process [J]. Materials Research Express, 2019, 6(9): 096593.

[27] QI Liang, ZHAO Ai-ming, ZHAO Zheng-zhi. Effect of rare earth La addition on microstructure and properties of Nb−Ti−Mo pipeline steel [J]. Transactions of Materials and Heat Treatment, 2012, 33(12): 82−87. (in Chinese)

[28] HU Bo-liang, WANG Kuai-she, HU Ping, ZHOU Yu-hang, YANG Fan, LI Qin-wei, CAO Wei-cheng, LIU Dong-xin, LIU Ren-zhi, YU Hai-liang. Effect of lanthanum in arc erosion of titanium−zirconium−molybdenum alloy [J]. Journal of Alloys and Compounds, 2017, 696: 522−528.

[29] KURZ W, FISHER D J. Fundamentals of solidification [M]. 4th ed. Zurich: Trans Tech Publications, 1998.

[30] CHENG B, CERIOTTI M, TRIBELLO G A. Classical nucleation theory predicts the shape of the nucleus in homogeneous solidification [J]. The Journal of Chemical Physics, 2020, 152(4): 044103.

[31] ZHANG Yi, GUO Xi-ping. Effect of CeO_2 on microstructure and oxidation resistance of silicide coatings prepared on Nb-silicide-based ultrahigh temperature alloy [J]. The Chinese Journal of Nonferrous Metals, 2013, 23(1): 99−107. (in Chinese)

[32] FERNANDES B B, RAMOS E C T, SILVA G, RAMOS A S. Preparation of Nb−25Si, Nb−37.5Si, Nb−66.6Si powders by high-energy ball milling and subsequent heat treatment [J]. Journal of Alloys and Compounds, 2007, 434: 509−513.

[33] LI Wei, YANG Hai-bo, SHAN Ai-dang, ZHANG Lan-ting, WU Jian-sheng. Effect of Mo addition on phase stability and high-temperature strength of $NbSi_2/Nb_5Si_3$ composites [J]. Materials Transactions, 2004, 45(12): 3282−3285.

镧对 $NbMoTiVSi_{0.2}$ 难熔高熵合金显微组织与力学性能的影响

徐 琴[1]，陈德志[2]，王聪锐[1]，曹文超[2]，王 琪[2]，崔洪芝[3]，张书彦[4]，陈瑞润[2,3]

1. 河南工业大学 机电工程学院，郑州 450001；
2. 哈尔滨工业大学 金属精密热加工国家级重点实验室，哈尔滨 150001；
3. 山东科技大学 材料科学与工程学院，青岛 266590；
4. 广东(东莞)材料基因高等理工研究院，东莞 523808

摘 要：为了研究 La 对难熔高熵合金显微组织与力学性能的影响，制备不同 La 含量的 $NbMoTiVSi_{0.2}$ 合金，并对其相组成、显微组织演变、压缩性能及相关机理进行系统分析。结果表明，不同 La 含量的合金由 BCC 固溶体、共晶组织、MSi_2 二硅化物和 La 析出相组成。共晶组织及大部分 La 析出相在晶界处形成，而二硅化物相在晶粒内部形成。La 的添加使合金晶粒形态由树枝晶转变为近等轴晶，且随着 La 含量从 0 增加到 0.5 at.%，合金的平均晶粒尺寸由 180 减小到 20 μm。压缩性能测试结果表明，由于晶界强化作用，合金的压缩强度和屈服强度均随着 La 含量的增加而增加；但是由于低强度 MSi_2 相的形成，其提高幅度有限。由于 La 析出相和脆性 MSi_2 相的形成，因此合金的韧性随着 La 含量的增加而降低。

关键词：高熵合金；镧；共晶组织；难熔金属；二硅化物

(Edited by Wei-ping CHEN)